The PHOBOS detector at RHIC

B.B.Back [a], M.D.Baker [b], D.S.Barton [b], S.Basilev [e], R.Baum [h], R.R.Betts [g], A.Białas [d], R.Bindel [h], W.Bogucki [c], A.Budzanowski [c], W.Busza [e], A.Carroll [b], M.Ceglia [b], Y.-H.Chang [f], A.E.Chen [f], T.Coghen [c], C.Connor [g], W.Czyż [d], B.Dąbrowski [c], M.P.Decowski [e], M.Despet [c], P.Fita [e], J.Fitch [e], M.Friedl [e], K.Gałuszka [c], R.Ganz [g], E.Garcia [h], N.George [a], J.Godlewski [c], C.Gomes [e], E.Griesmayer [e], K.Gulbrandsen [e], S.Gushue [b], J.Halik [c], C.Halliwell [g], P.Haridas [e], A.Hayes [i], G.A.Heintzelman [b], C.Henderson [e], R.Hollis [g], R.Hołyński [c], D.Hofman [g], B.Holzman [b], E.Johnson [i], J.Kane [e], J.Katzy [g,e], W.Kita [c], J.Kotuła [c], H.Kraner [b], W.Kucewicz [g], P.Kulinich [e], C.Law [e], M.Lemler [c], J.Ligocki [c], W.T.Lin [f], S.Manly [i,j], D.McLeod [g], J.Michałowski [c], A.Mignerey [h], J.Mülmenstädt [e], M.Neal [e], R.Nouicer [g], A.Olszewski [c,b], R.Pak [i,b], I.C.Park [i], M.Patel [e], H.Pernegger [e], M.Plesko [e], C.Reed [e], L.P.Remsberg [b], M.Reuter [g], C.Roland [e], G.Roland [e], D.Ross [e], L.Rosenberg [e], J.Ryan [e], A.Sanzgiri [j], P.Sarin [e], P.Sawicki [c], J.Scaduto [b], J.Shea [h], J.Sinacore [b], W.Skulski [i], S.G.Steadman [e], G.S.F.Stephans [e], P.Steinberg [b], A.Strączek [c], M.Stodulski [c], M.Stręk [c], Z.Stopa [c], A.Sukhanov [e], K.Surowiecka [c], J.-L.Tang [f], R.Teng [i], A.Trzupek [c], C.Vale [e], G.J.van Nieuwenhuizen [e], R.Verdier [e], B.Wadsworth [e], F.L.H.Wolfs [i], B.Wosiek [c], K.Woźniak [c,b], A.H.Wuosmaa [a], B.Wysłouch [e], K.Zalewski [d], P.Żychowski [c]

(The PHOBOS Collaboration)

[a] *Physics Division, Argonne National Laboratory, Argonne, IL 60439-4843*

[b] *Chemistry and Collider-Accelerator Departments, Brookhaven National Laboratory, Upton, NY 11973-5000*

[c] *Institute of Nuclear Physics, Kraków, Poland*

[d] *Department of Physics, Jagellonian University, Kraków, Poland*

[e] *Laboratory for Nuclear Science, Massachusetts Institute of Technology,*

Cambridge, MA 02139-4307

[f] *Department of Physics, Central National University, Chung-Li, Taiwan*

[g] *Department of Physics, University of Illinois at Chicago, Chicago, IL 60607-7059*

[h] *Department of Chemistry, University of Maryland, College Park, MD 20742*

[i] *Department of Physics and Astronomy, University of Rochester, Rochester, NY 14627*

[j] *Department of Physics, Yale University, New Haven, CT 06520*

Abstract

This manuscript contains a detailed description of the PHOBOS experiment as it is configured for the Year 2001 running period. It is capable of detecting charged particles over the full solid angle using a multiplicity detector and measuring identified charged particles near mid-rapidity in two spectrometer arms with opposite magnetic fields. Both of these components utilize silicon pad detectors for charged particle detection. The minimization of material between the collision vertex and the first layers of silicon detectors allows for the detection of charged particles with very low transverse momenta, which is a unique feature of the PHOBOS experiment. Additional detectors include a time-of-flight wall which extends the particle identification range for one spectrometer arm, as well as sets of scintillator paddle and Čerenkov detector arrays for event triggering and centrality selection.

Key words: Relativistic heavy ion collisions, Si detectors

1 Introduction

PHOBOS is one of the initial suite of four detectors currently installed at the Relativistic Heavy Ion Collider (RHIC) at Brookhaven National Laboratory. Heavy ion collisions at nucleon-nucleon center-of-mass energies ($\sqrt{s_{NN}}$) of 130 GeV are believed to have produced the highest energy density over an extended volume ever achieved in a laboratory setting [1–4]. According to the fundamental theory of strong interactions, quantum chromodynamics (QCD), the deconfinement and chiral symmetry restoration [5] expected at these high energy densities will lead to new physics phenomena.

Detector design for relativistic heavy ion collisions is a particular challenge since they yield the highest number of charged particles, and therefore the highest density of particle trajectories ever seen in the laboratory. In addition, the PHOBOS research program and detector design were based on the premise that the signatures of new physics were *a priori* unknown. This uncertainty led to the primary goal of studying the collisions, at least initially, by triggering on almost all inelastic collisions and detecting nearly all charged particles over a broad range of transverse momentum, p_T, and pseudo-rapidity, η, using a multiplicity detector.

In order to learn more about the dynamical evolution of nucleus-nucleus collisions and to study potential new physics phenomena, the detector also includes a two-arm Spectrometer which permits a detailed analysis of about 2% of the particles produced in each collision. This study is focused on particles emitted near mid-rapidity ($0 \leq \eta \leq 2$) in two opposite azimuthal angle (ϕ) slices of 0.2 radians each. This choice of focus was dictated by the following considerations: 1) The highest energy densities and any new physics effects are expected to occur near mid-rapidity. 2) A goal is to study particles down to very low p_T, both to cover the phase space completely, and because large-volume physics effects may be manifested at low p_T. The acceptance of the Spectrometer is therefore optimized for detecting low p_T particles. This study also requires a thin Beryllium beam pipe to minimize energy loss, multiple scattering, and secondary production for these low p_T particles. 3) The two Spectrometer-arm design optimizes the two-particle acceptance in phase space, especially for Hanbury-Brown and Twiss analysis, detection of very low p_T ϕ-meson decays, and back-to-back high p_T particles. 4) Particle identification for $p_T < 1$ GeV/c, where the majority of the particle production is expected to occur, is achieved by measuring the average energy loss in the silicon detectors that are used also to determine the particle trajectory in the magnetic field.

Aside from being of unknown signature, the new physics phenomena may occur only in rare events. The detector was therefore designed to operate at a high trigger rate, allowing an offline search for unusual events or rare fluctuations which might signal a phase transition or critical point.

The key features of the PHOBOS design reflect a balance between these physics goals and the physical and financial constraints. The coverage, almost eleven units of pseudorapidity, is restricted by the beam pipe diameter and the location of RHIC accelerator elements upstream and downstream of the detector. The minimum p_T cutoffs of 10 MeV/c for detectable, and 30 MeV/c for momentum analyzed particles are determined by the wall thickness of the Beryllium beam pipe. The maximum p_T for particle identification is determined primarily by the flight path to the time-of-flight counters allowed by the tunnel walls and reasonably achievable time-of-flight resolution. The detector is rather compact; almost all elements are located within 1 m of the beam line with the first detectors located in the closest proximity to the interaction region. This minimizes the effect of particle decays and multiple scattering in material near the collision region, which is especially important at low p_T.

Despite the deliberate emphasis on low p_T, the detector is capable of measuring momentum (although not the particle type) at high p_T near mid rapidity -

a region of phase space which includes effects of hard processes (minijets, jet quenching etc.).

2 The PHOBOS detector

The PHOBOS detector, illustrated in Fig. 1, consists of four subsystems: a Multiplicity array, a Vertex detector, a two-arm magnetic Spectrometer including a time-of-flight wall, and several trigger detectors which also determine the centrality of collisions.

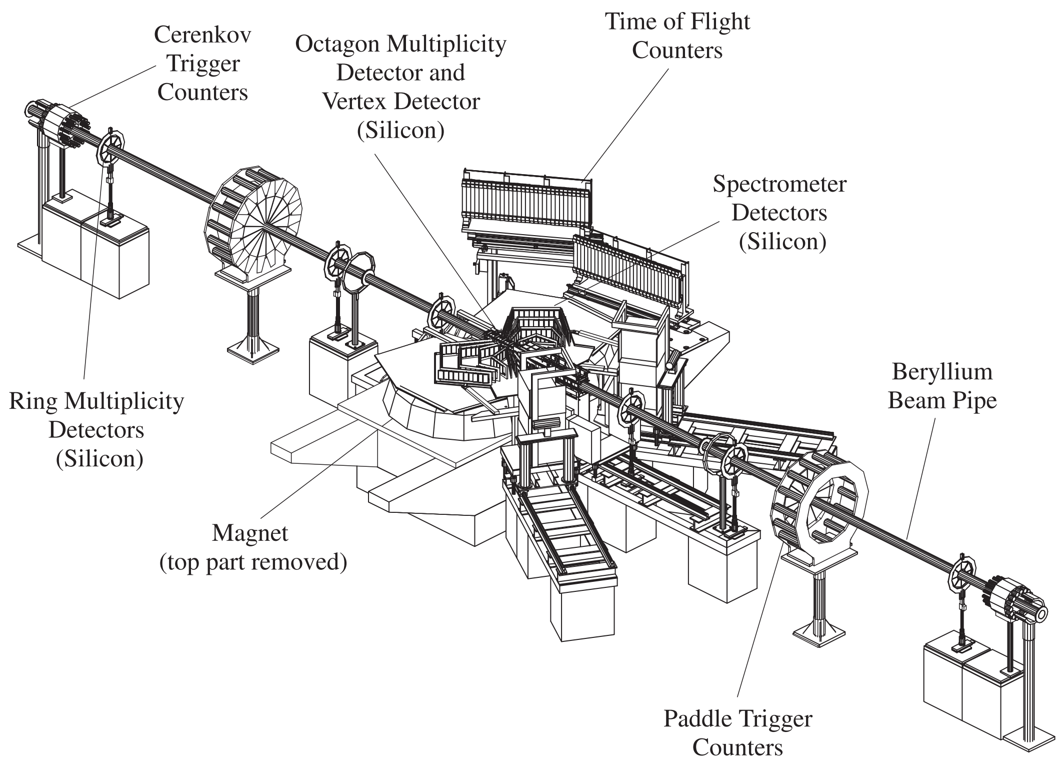

Fig. 1. Schematic layout of the PHOBOS detector. The top yoke of the magnet is not shown.

The beam pipe consists of three segments of Be tubing, each 4 m long, 76 mm in diameter with a wall thickness of ≈1.0 mm. The PHOBOS coordinate system has its origin at the nominal interaction point, the z-axis along the beam line into the magnet (left in Fig. 1), the y-axis is vertical, and the x-axis in the horizontal plane on the TOF-wall side of the beam line to form a right handed system.

The Multiplicity array is a single layer of silicon detectors that is used to measure the number and angular distribution of charged particles emitted from the collisions over a pseudo-rapidity range of $|\eta| \leq 5.4$. It consists of a central, octagon-shaped section covering $|\eta| < 3.2$ and six ring detectors located at distances of ±1.13, ±2.35, and ±5.05 m from the interaction point along the beam axis, which extend the pseudorapidity coverage to $|\eta| \leq 5.4$ (see Fig. 2).

Above and below the interaction region, double layers of finely segmented Si sensors are used for vertex determination. The geometrical acceptances of the Octagon, Rings and the inner layer of the Vertex detector are shown in Fig. 2. Aside from the two openings for the Spectrometer arms these detectors provide almost complete azimuthal coverage for $|\eta| < 5.4$.

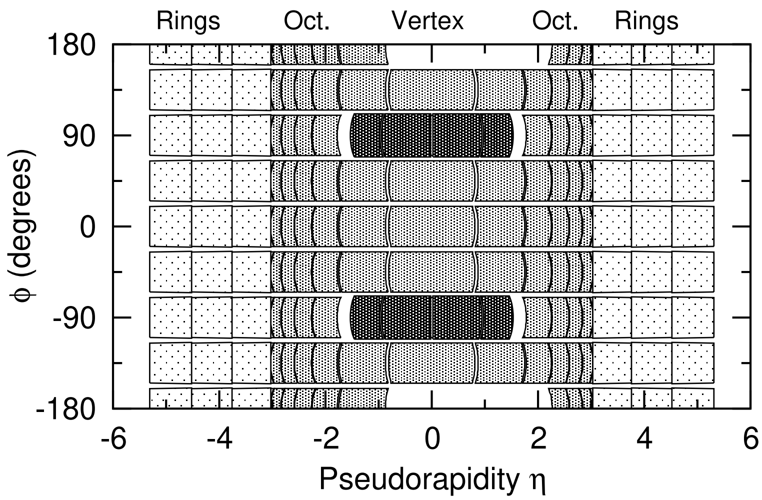

Fig. 2. The geometrical acceptances of the Ring (light), Octagon (medium) and Inner Vertex (dark) detectors for particles emitted from the nominal interaction point are shown as a function of η and ϕ.

The Spectrometer consists of two arms of 15 silicon layers each, located on either side of the beam axis. This subsystem provides tracking and particle identification of roughly 2% of the charged particles emitted in a typical interaction. It covers a span of ≈0.7 units of pseudorapidity for a given vertex location with a total coverage of approximately $0 \leq \eta \leq 2$. Charged particle tracking starts ≈100 mm from the beam axis and extends for a distance of ≈750 mm. The orientation of the Spectrometer was designed to allow tracking of very low p_T particles. The dimensions of the silicon sensor pads range from ≈0.4 mm to 1.0 mm in the bend direction. Additional segmentation in the vertical direction is provided. Particle identification is achieved using the energy loss (dE/dx) measured in each Si layer. Two arrays of scintillator time-of-flight (TOF) counters, each containing 120 slats, extend the particle identification capabilities to higher momenta in one spectrometer arm.

The PHOBOS magnet is a double dipole structure with the field in opposite directions on the two sides. The pole tips are shaped such that the first few planes of the Spectrometer reside in a very low field region, while the subsequent detector planes are placed in a roughly constant vertical field of 2 T. The straight line tracks obtained from detectors in the low field region serve as seeds for the more complicated algorithm used to reconstruct the curved tracks in the magnetic field region.

The primary event trigger is provided by a coincidence between two sets of 16 scintillator paddle counters located at ±3.21 m from the nominal interaction point along the beam axis and covering $3 < |\eta| < 4.5$. The time difference measured between hits in the counters is restricted to ensure that the collision occurred near the center of the interaction region. The sum of the measured signals of these counters is also used to estimate event centrality. Additional triggering, multiplicity, and vertex location information is provided by the array of 16 Čerenkov radiators located near the end of the Beryllium beam pipe sections.

Zero-degree calorimeters (ZDCs, not shown in the figure)[6] located ±18.5 m from the nominal interaction point are nearly identical for each of the four RHIC experiments. These counters provide a common means to measure luminosity and centrality using the beam-velocity neutrons from fragmentation of the colliding nuclei.

3 The PHOBOS magnet

The PHOBOS magnet is a conventional room-temperature magnet of a double dipole design. The magnet straddles the beam-pipe near the collision point with one magnet dipole located on each side of the beam pipe. The two dipoles are in a series magnetic circuit, providing vertical fields of opposite polarity in the two arms. The total bending power of the magnet is ≈1.5 Tm. An isometric view of the magnet is shown in Fig. 3.

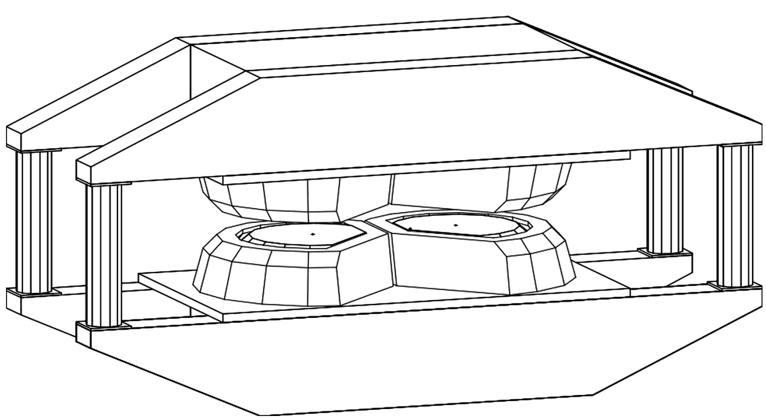

Fig. 3. Perspective view of the PHOBOS magnet. The beam pipe runs through the middle of the magnet.

The magnet pole gap is 158 mm with coils unenergized. Under full power (nominally 342 kW) and full magnetic field (2.18 T maximum gap field) the yoke deflection is about 2 mm. The four pole pieces are of cylindrical "double-taper" design, with the addition of two "cuts", one vertical and one at 12° to the vertical in order to provide the necessary low and high field regions. The total magnet weight is about 45 tons.

The four coils are driven in a series-parallel configuration (the upper two coils in one series electrical circuit, the lower two coils in another electrical circuit) from a power supply providing up to 115 VDC at 3600 A. The voltage drop across each coil is $0.0264\ \Omega \times 1800\ \mathrm{A} = 47.5$ V, giving a total voltage drop of 95 V for the series circuit. Resistive heating losses within the conductors are dissipated by water cooling.

An LC-circuit filters the output current of the power supply. The remaining ripple is less than 0.1%. The filter causes an additional voltage drop of 10 V at maximum load. The magnet is intended for continuous operation. It was designed at MIT and built by Danfysik, Denmark.

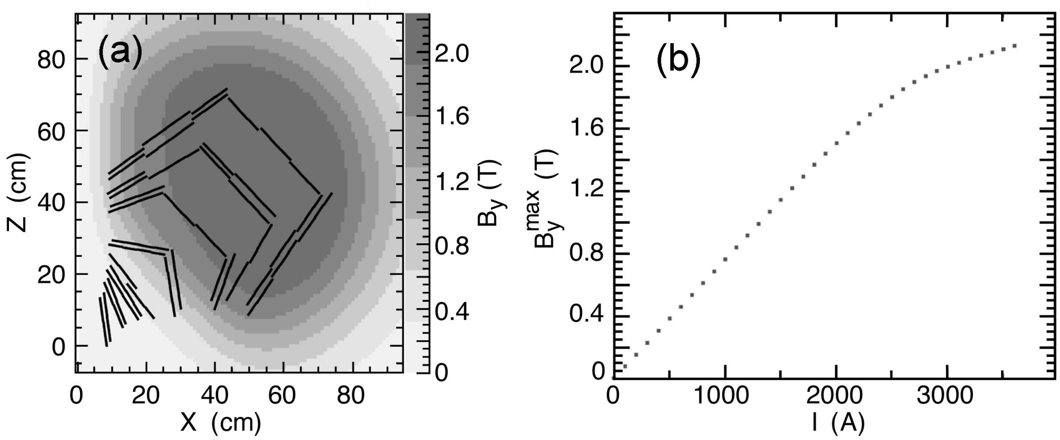

Fig. 4. a) B_y component of the magnetic field in the mid-plane as a function of the x and z coordinates. In the PHOBOS coordinate system the beam line is located along z, at $x = y = 0$. The outlines of the Spectrometer silicon detectors are also indicated. The maximum magnetic field is 2.18 T. b) The maximum B_y component is shown as a function of excitation current. The nominal excitation current is 3600 A.

3.1 Magnetic Field

The magnetic field region was measured at a current of 3600 A at 15120 nodal points. The points were surveyed to a precision of about 150 μm in the PHOBOS coordinate system. Tilt angles of the Hall-probes were monitored during mapping and the field components were subsequently corrected for any such misalignments. The final uncertainty in the processed magnet field map is smaller than 0.7 %. Figure 4.a shows the vertical component, B_y, of the measured magnetic field in the mid-plane of the gap for one of the two arms at the nominal excitation current of 3600 A. Also indicated is the location of the silicon Spectrometer planes in the gap. The B_y component rises from zero field to the full 2.18 T field at about 400 mm from the beam axis, and remains relatively constant within the pole tips. The B_x and B_z components are less than 0.05 T in the same region. The B_y component of the field is shown as a function of the current in Fig. 4b. The yoke iron starts saturating at a current of about 2500 A.

4 Silicon Sensor Technology

The PHOBOS apparatus makes extensive use of silicon pad detector technology. Nine different wafer designs were used to meet requirements for particle tracking, vertex finding and particle multiplicity measurements. A summary of the physical characteristics of the Si sensors is given in Table 1. Although the pad sizes and shape vary greatly among the different components, a common AC-coupled, single sided, silicon pad design was used for all sensors. The junctions are biased by 5 MΩ polysilicon resistors. The signals are AC coupled through a coupling capacitor consisting of a 0.2 μm oxide nitride oxide (ONO) layer and the first metal layer. On top of the first metal layer there is a 1.2 μm ONO dielectric layer which carries the second metal signal traces to the bonding pads at one edge of the sensor. This design makes it possible to glue a hybrid board (see Sect. 4.3) to the edge of the sensors and minimizes the amount of material in the active detector area. See Ref. [7] for details.

4.1 Production and testing

The sensors were produced by the Miracle Technology Co. in Taiwan under supervision of National Central University (NCU). Wafers with thicknesses between 300 and 340 μm, a specified active area leakage current and polysilicon resistor value were selected and diced to the desired detector size. After dicing, more detailed measurements were performed on the sensor and test keys fabricated on the same Si wafer as the sensor. The tests were carried out using a probe station under control of a PC running LabView [8] data analysis software. The measured characteristics included: 1) Depletion voltage obtained by measuring the capacitance of a simple *pn* junction with guard ring as a function of bias voltage. 2) Leakage current of the active sensor area. 3) Polysilicon resistor values obtained by measuring eleven polysilicon resistors identical to the ones used on the sensors.

Table 1
Physical characteristics for the PHOBOS silicon pad sensors

Detector System	Sensor Type	Active Area [mm^2]	Number of Pads	Pad Size [mm^2]
Spectrometer	1	70.000 x 22	70 x 22	1.000 x 1.0
	2	42.700 x 30	100 x 5	0.427 x 6.0
	3	42.688 x 60	64 x 8	0.667 x 7.5
	4	42.688 x 60	64 x 4	0.667 x 15.0
	5	42.688 x 76	64 x 4	0.667 x 19.0
Multiplicity	Octagon	34.880 x 81.280	30 x 4	2.708 x 8.710
	Ring	$\approx$ 3200	64	$\approx$ 20 - 105
Vertex	Inner	60.584 x 48.180	4 x 256	0.473 x 12.035
	Outer	60.584 x 48.180	2 x 256	0.473 x 24.070

In addition, the sensors were scanned for anomalous capacitance values at 0, 50 and 100 V bias and the results compared to standard templates for each sensor type since the capacitance depends on the detailed geometry of the readout traces [9]. Short circuits in the coupling capacitors caused by pinholes in the dielectric layer were identified by applying 5 V on each channel bonding pad and measuring the current flowing from this bonding pad, through the coupling capacitor, into the bias circuitry.

Silicon sensors selected for mounting onto detector modules were required to fulfill the following electrical specifications: 1) full depletion voltage less than 70 V, 2) active area leakage current less than 5 μA for Vertex and Spectrometer sensors, less than 10 μA for Octagon and Ring sensors, 3) polysilicon resistor value between 1 and 10 MΩ and 4) less than 3% broken channels.

About 2000 Si wafers were manufactured and tested. About half of these were Spectrometer sensors of various types, the other half were Multiplicity and Vertex sensors. Fig. 5 summarizes the distributions of the most important operating characteristics of the sensors used for the tracking Spectrometer.

4.2 Module assembly and testing

The Silicon sensors were assembled into different module types. A module consists of one or more sensors glued to one or two hybrid boards, which physically support the sensors and carry the preamplifier chips and associated circuitry

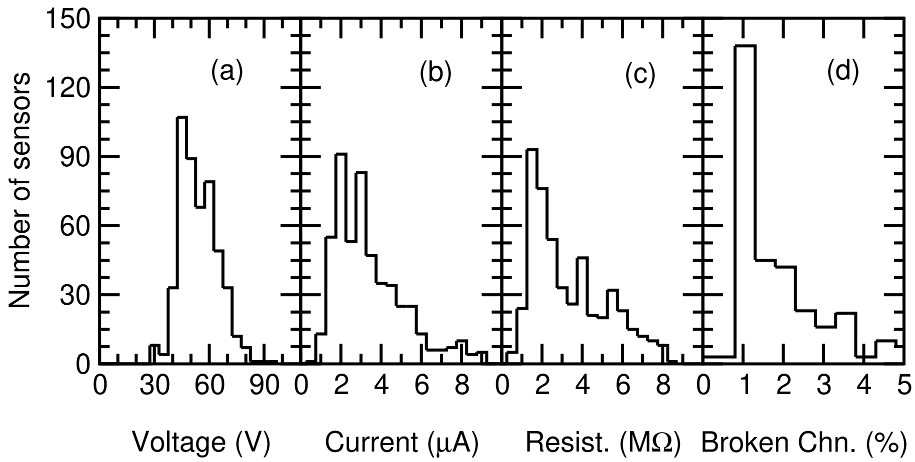

Fig. 5. Distributions of the most important characteristics of the Spectrometer sensors. (a) Bias voltage at full depletion, (b) active area leakage current, (c) polysilicon resistance, and (d) percentage of broken channels.

used to read out the detector signals. The hybrid circuits are described in more detail in Sect. 9. In total, thirteen different hybrid designs are used in the PHOBOS detector. Photographs of four module types are shown in Fig. 6.

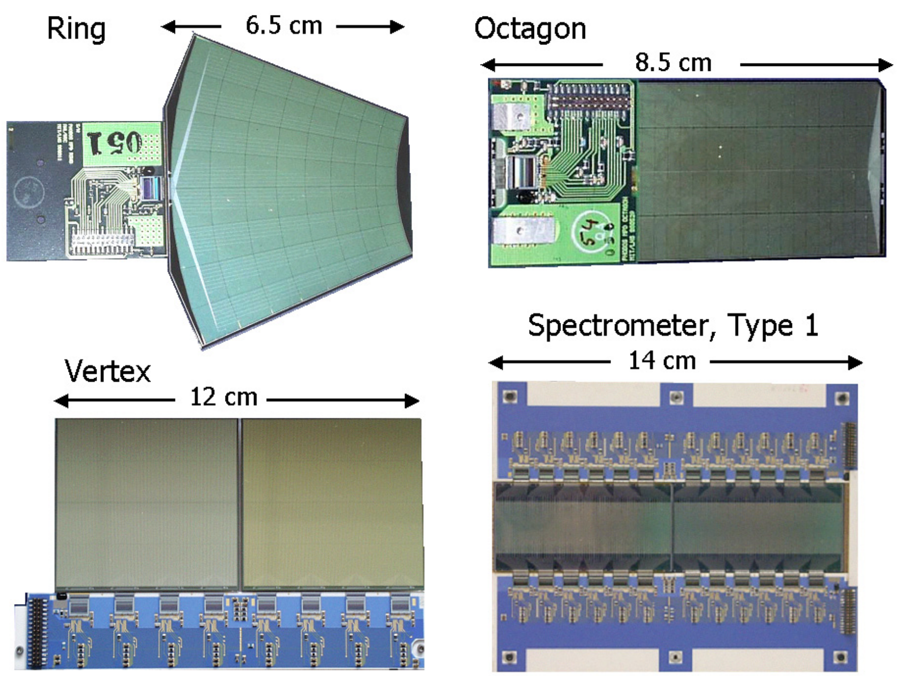

Fig. 6. Photographs of different detector modules.

Spectrometer and Vertex modules contain two to four sensors each. The large number of channels on these sensors require several preamplifier/shaper chips for the readout. The most complicated detectors are those in the first layers of the Spectrometer which use two Type 1 sensors with 1536 channels each read out by 24, 128-channel VA chips. The large number of chips on the

Spectrometer and Vertex detectors requires a ceramic hybrid design with thick film circuitry to withstand the heat load. The Silicon wafers are glued to the ceramic hybrid via a glass strip of "L"-shaped cross section. To avoid tracking efficiency loss in the Spectrometer, the sensors overlap resulting in a complicated assembly procedure. A special gluing station was constructed for the assembly of these modules. The hybrid boards used for Octagon and Ring modules were fabricated from ordinary 0.7 mm thick printed circuit boards glued directly onto the Si wafer using a special gluing station.

Electrical connections between the VA chips and the silicon sensors and hybrid circuits were made with micro wire bonds, performed at MIT and by the Silicon-detector group at Fermi National Accelerator Laboratory. The hybrids were populated with chips and the functionality of all channels verified before final assembly into modules. Malfunctions were, in most cases, due to wire bonding problems which could usually be repaired. After the sensors were mounted the whole module was again tested and noise, gain and pedestal were measured for each channel. An electron source was used to determine the signal-to-noise ratio for minimum ionizing particles.

The results of the ≈ 3 million test measurements were entered into an automated database utilizing Oracle [10] software. These results are available to all online, offline and control software and are used to set optimal operating parameters for each module separately and to generate mapping files which include information about the location of broken and noisy channels.

4.3 Energy resolution of Si detectors

The energy resolution of the silicon detector modules is extremely important for the physics goals of PHOBOS. In the Spectrometer modules, the average deposited energy in detector pads along a charged particle track is used for particle identification in conjunction with measured momentum obtained from the curvature of the track in the magnetic field region. In the multiplicity detectors (Octagon and Rings) the deposited energy, when corrected for track length in the silicon, is used to determine the number of tracks traversing a given pad to obtain the charged particle multiplicity.

For the data analysis that relies on counting the number of hits in a silicon detector the energy resolution is important for discriminating between detector noise and single particle hits. The overall ratio of the location of the peak for minimum ionizing particles (MIP) to the detector RMS noise is shown in Fig. 7 for the nine different silicon wafer types. As expected there is a clear correlation between the Signal-to-Noise ratio and the pad sizes (See Table 1), such that the sensors with the largest pad sizes (Octagon and Rings) exhibit

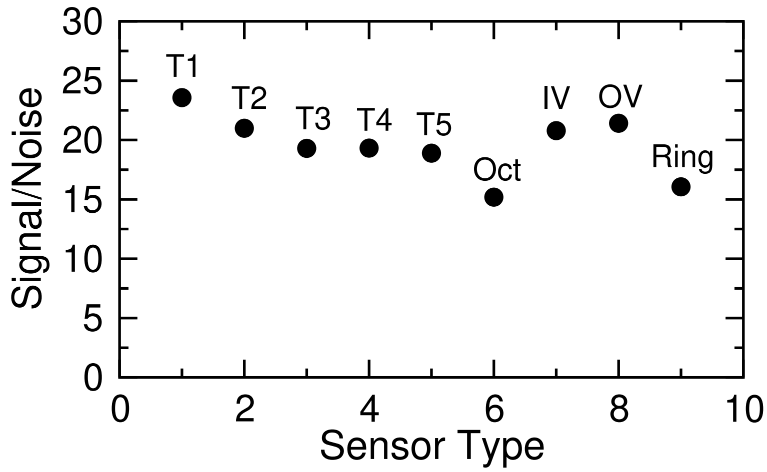

Fig. 7. Signal (MIP peak) to noise (RMS) is shown for all nine detector types.

the smallest values of $S/N \approx 16$ whereas the Type 1 sensors, with pad sizes of only 1 mm^2, have the highest values of $S/N \approx 24$. In all cases the design goal of $S/N > 12$ is comfortably exceeded. Additional details on the silicon detector performance are given in Ref. [11].

5 Silicon Detector Subsystems

5.1 Multiplicity array

The role of the PHOBOS multiplicity array is to determine, on an event-by-event basis, the number of charged particles emitted from a heavy-ion collision as a function of both η and ϕ over the entire available solid angle. The measurement is performed by recording the energy deposited by charged particles in an array of silicon pad detectors that effectively encloses the beam pipe, covering nearly all of 4π. The multiplicity array consists of the Octagon and the six Ring detectors. Isometric drawings of the Octagon and of a Ring detector are shown in Fig. 8.

5.1.1 Octagon

The Octagon detector contains 92 silicon pad detectors in a 1.10 m long, 90 mm (face to face) diameter barrel surrounding the beam pipe in the mid-rapidity region. The silicon pad detectors are mounted in 8 faces, each containing up to 13 sensors. In the regions immediately surrounding the interaction point, sensors are removed from the faces directly in front of the Spectrometer arms, and the Vertex detectors to allow for unimpeded acceptance of these other detector systems (see Fig. 2). Each sensor is 84 mm in length and 36 mm wide, with the active area divided into 120 pads arranged in four rows of 30 pads each, running along the z direction. The pad arrangement was chosen to optimize the expected occupancy, η coverage, and to minimize the readout complexity. The pads on each sensor are read out with a single 128-channel preamplifier/shaper chip (see Sect. 9). Eight of these channels are connected to test structures on the sensor to monitor the noise and baseline response.

The η coverage of individual Octagon pads ranges from approximately $\Delta\eta$=0.06 units at mid rapidity to $\Delta\eta$=0.005 units at the ends of the Octagon. About 95% of the area of each Octagon sensor is active and the gaps between them are 1 mm wide. The total active area of the Octagon, not including the sensors removed in front of the Spectrometer and Vertex detectors, is thus approximately 89% of the total area subtended.

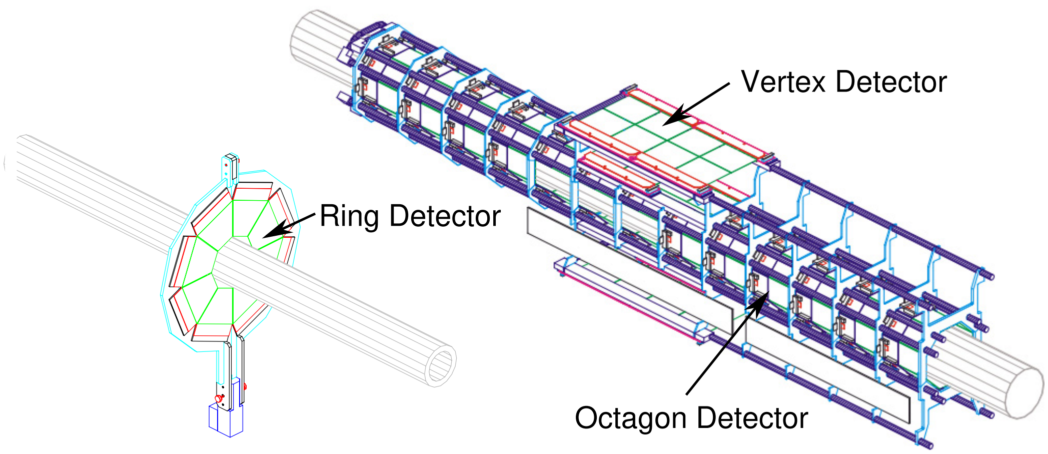

Fig. 8. Isometric drawing of the Octagon frame with detector modules and a complete Ring detector.

The Octagon support structure is constructed of a light-weight Aluminum frame, see Fig. 8. Part of the Octagon frame is fabricated from Aluminum tubes, through which chilled water is circulated in order to cool the readout electronics chips affixed to each sensor. The low-Z, low mass frame minimizes the amount of material near the collision point in order to limit secondary particle production and multiple scattering. The frame also supports printed circuit boards and flexible multi-conductor cables which carry the signals from each detector to the rest of the readout electronics. Finally, the Octagon frame also supports the two-layer Vertex tracking detectors (see Sect. 5.2).

A small sample of data obtained with the Octagon is shown in Fig. 9. Peaks corresponding to one and two minimum ionizing particles traversing a single detector pad are clearly visible.

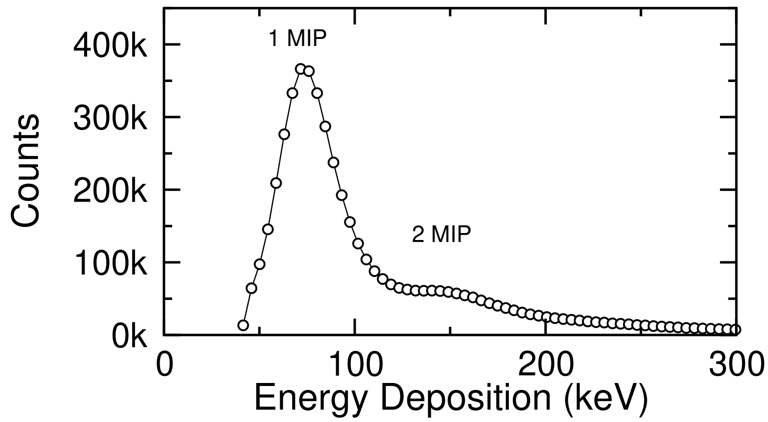

Fig. 9. Energy deposition spectrum for the Octagon detector. Data were obtained from Au+Au collisions at $\sqrt{s_{NN}}$=130 GeV. The spectrum has been corrected for the angle of incidence.

5.1.2 Rings

The η coverage of the Octagon is augmented by six octagonal Ring arrays of silicon pad detectors as described above. Each Ring detector consists of eight trapezoidal silicon pad sensors containing 64 pads, which are arranged into 8 radial columns and 8 rows. The pad sizes range from approximately 3.8mm $\times$ 5.1 mm at small radii, to 10.2 mm $\times$ 10.2 mm at the largest radii, with the specific sizes chosen such that each pad subtends an approximately equal η range ($\Delta\eta \approx 0.1$) for collisions occurring near the nominal interaction point. Each Ring module is read out by a 64-channel preamplifier-shaper chip. The inner diameter of each Ring is 100 mm, and the outer diameter 220 mm. The radial gaps between the sensors in each Ring are 1 mm wide.

The Ring modules are mounted on carbon-fiber frames, which also support the printed circuit boards used to carry the signals from each module to the readout cables. This construction minimizes the amount of high-Z material intersected by particles traveling to downstream Rings and trigger detectors (see Sect. 7).

5.2 Vertex Detector

The design goal for the Vertex detector is to determine the vertex position with an accuracy of better than 0.2 mm in the z-direction (along the beam line) for central collisions that take place within $\pm$100 mm of the nominal center of the apparatus. To achieve this goal, two sets of finely segmented silicon pad detectors are installed on the Octagon frame, above and below the beam line centered at z=0. Each set consists of two layers of sensors (the “Inner” and “Outer” Vertex detectors). These arrays of sensors are used to identify two-point tracks from hits in the two layers, which point back to the original collision vertex. In addition, the Vertex detectors are used in the determination of the charged particle multiplicity within their solid angle coverage. The Inner Vertex detectors consist of two modules, each with two sensors that are divided into four columns of 128 pads (see Sect. 4), and are located 56 mm above the beam axis. These detectors cover almost the same solid angle as the six Octagon modules that were removed from the Octagon in this region, (see Fig. 2). The pad characteristics of the Vertex detector are listed in Table 1. The Outer Vertex detectors consist of four detector modules, each with two sensors, each divided into two columns of 128 pads, and are mounted above and below the Inner Vertex detectors at a distance of 118 mm from the nominal beam axis. The pad sizes are made small enough to obtain good pointing resolution, and a low occupancy factor for even the highest multiplicity events.

The η coverage of the Inner Vertex detectors is approximately $|\eta| < 1.54$, and of the Outer Vertex detectors $|\eta| < 0.92$ for collisions at $|z| = 0$. The azimuthal coverage provided by each Inner/Outer Vertex array is $\Delta\phi = 42.7°$.

The accuracy of the vertex determination is important for several types of measurements with the PHOBOS apparatus. For example, the location of the identified vertex is used as an anchor for the tracking in the Spectrometer arms. Several effects contribute to the accuracy of the vertex determination, the most important of which are the 1) pad sizes of the Inner Vertex sensors, 2) multiple scattering in the beam pipe and the Inner Vertex sensors 3) inaccuracies of the measured positions of sensors in space, and 4) the multiplicity of the event. The Vertex sensors have a pitch between pads in the beam (z) direction of 473 μm and the Inner and Outer Si sensors are located 56 and 118 mm from the interaction point, respectively. This gives a contribution to the vertex resolution of about $450/\sqrt{N-1}$ μm, where N is the number of tracks. For comparison, the contribution from multiple scattering for 0.5 GeV pions in the beam pipe and the Inner Vertex detector is $\approx 50/\sqrt{N-1}$ and $70/\sqrt{N-1}$ μm, respectively resulting in an overall multiple scattering contribution of $\approx 85/\sqrt{N-1}$ μm.

The largest contribution to the vertex resolution for high multiplicity events comes from the inaccuracy in the measurements of the actual geometrical positions of the sensors. The survey of the sensors mounted on the support frame was incomplete since the Inner Vertex sensors were obscured by other components of the PHOBOS detector. An initial measurement of the vertex resolution using the survey geometry was obtained by comparing z-positions obtained from the top and bottom Vertex detectors independently. This comparison gave a result of $\Delta z \approx 320\mu$m, for minimum bias Au+Au collisions at $\sqrt{s_{NN}}$=130 GeV (see Fig. 10) indicating that the main contribution to the z-vertex resolution stems from the sensor misalignment. Successive re-adjustments of the sensor alignment using cosmic ray tracks that traverse all

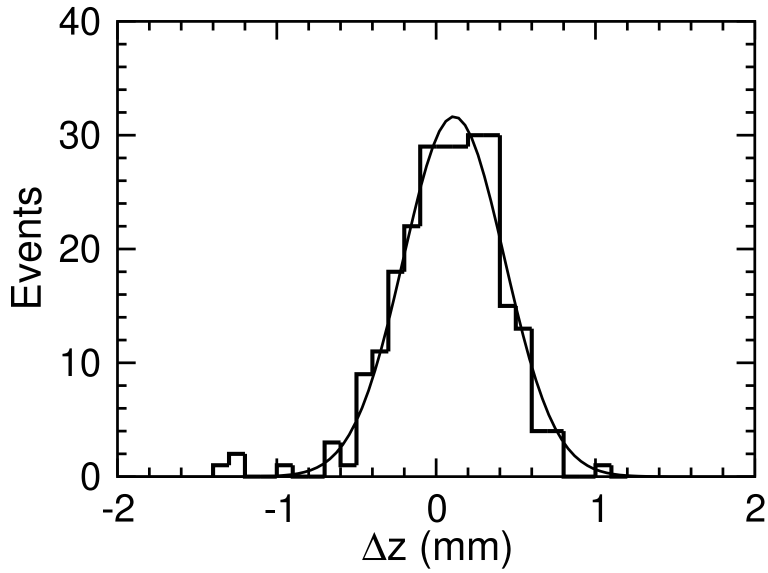

Fig. 10. The difference, Δz, between the vertex positions along the beam axis obtained from the top and bottom Vertex detectors (solid histogram). The curve represents a Gaussian fit to the data.

four Vertex detector layers will improve the vertex resolution significantly.

The vertex position was also measured using the first Si detector planes of the Spectrometer arms. Similar accuracies were obtained although noticeable shifts between the two detector systems have been observed indicating a small misalignment of the two detector systems.

5.3 Tracking Spectrometer

The PHOBOS Spectrometer consists of two arms, located on opposite sides of the beam line. Each arm has 137 sensors and 780 readout chips assembled into 42 multi-sensor modules accomodating a total of 56064 channels. The modules are mounted on 8 Aluminum water-cooled frames that are attached to a carrier plate as shown in Fig. 11. The first three frames are in an essentially field-free region, one frame is in the transition field and the four largest frames are located in the 2 Tesla field region (see Fig. 4).

The carrier plates are supported at three points that are not mechanically connected to the magnet. The maximum deflection of the plate is less than 300μm. The carrier plates were fabricated from a non-conductive carbon-epoxy material to minimize vibrations caused by the ripple in the magnet current. Magnet field crash tests (instantaneous switching off of the magnet current) produced no noticeable movement of the Spectrometer arms. A prototype design using Aluminum material proved unacceptable because of excessive vibrations in the magnetic field - presumably caused by induced eddy currents

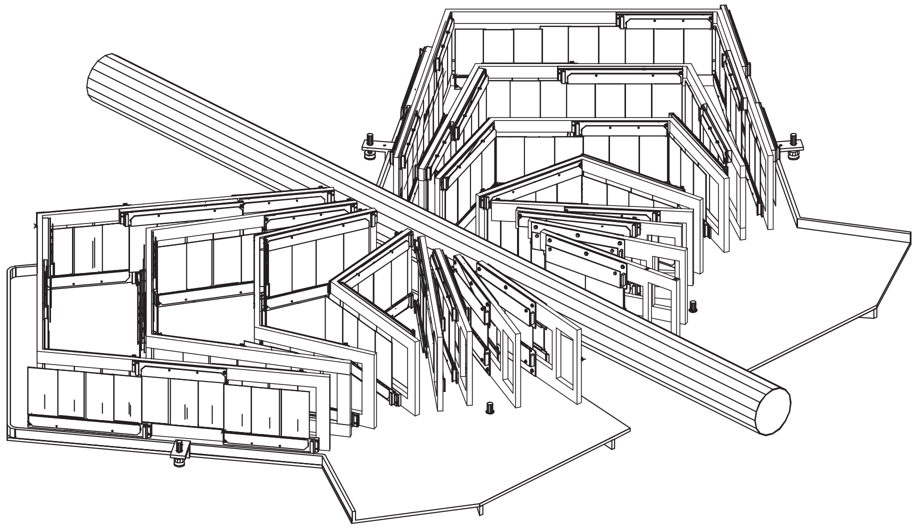

Fig. 11. Isometric diagram of the Si detector planes of the tracking Spectrometer.

in the conducting plate. The entire magnet gap has a light and air tight enclosure. This enclosure is continually flushed with dry nitrogen to ensure that the relative humidity is less than 10%.

5.3.1 Geometrical acceptance

The geometrical acceptance of the tracking Spectrometer depends on a combination of the vertex position, the position of the silicon detectors, the magnetic field profile and the number of detector planes required for identifying and measuring the momentum of particles accepted into the Spectrometer. The regions in rapidity, y, and p_T for which pions, kaons and protons are accepted into the Spectrometer are indicated by solid contour curves in Fig. 12. The geometric acceptance extends to $p_T \to \infty$, but upper p_T limits exist for identified particles as discussed in Sect. 5.3.2. In order to account for the fact that not all Si layers are fully equipped with sensors, particle trajectories were required to traverse twelve of the fifteen Silicon layers in the Spectrometer and originate from a collision vertex within the range $-100 < z < 100$ mm.

5.3.2 Particle identification

Particle identification in the Spectrometer relies on energy-loss, momentum, and time-of-flight measurements. In the low momentum region ($p_\pi < 55$ MeV/c, $p_K < 135$ MeV/c, and $p_p < 225$ MeV/c) the energy loss depends strongly on the velocity of the particles, and whether the particle stops in one of the first seven silicon planes. The stopping particle can be identified using its measured energy deposition in the detector plane(s) and its total energy (obtained by summing all the energy depositions). For higher momentum

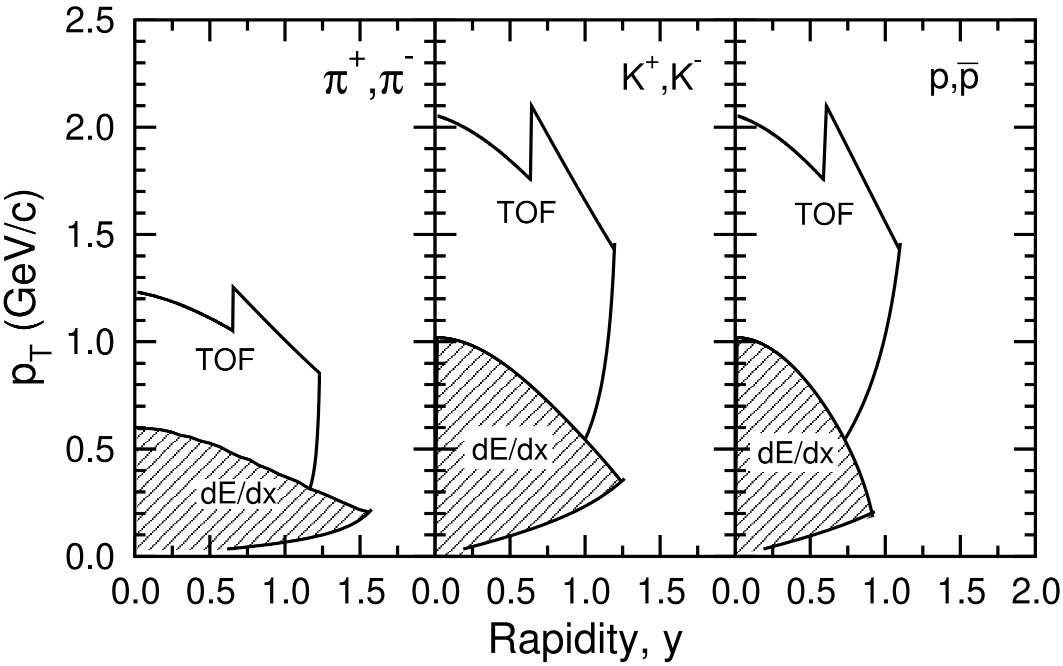

Fig. 12. Acceptance regions in rapidity and transverse momentum for pions, kaons and protons. The various regions are labeled according to the technique that is be used to achieve particle identification. The "saw-tooth" structure at high p_T is a result of the segmentation of the time-of-flight wall.

particles that traverse all silicon detector planes within the magnet gap the momentum can be determined from the measured radius of curvature. A measurement of the energy deposition combined with the results of a momentum analysis can be used for particle identification in this regime. This technique allows K/π separation up to about 600 MeV/c and p/K separation up to about 1.2 GeV/c at mid-rapidity, (see Fig. 12), corresponding to an energy resolution of about 4% and a 3σ limit requirement on the energy deposition. Particles with momenta above these values can be identified on the basis of their momentum and their time-of-flight obtained from the time-of-flight wall located behind one of the magnetic Spectrometer arms. Using the time-of-flight information, and requiring more than 400 ns time-of-flight difference between neighboring particle species, the range of π/K separation is extended to about 1.2-1.4 GeV/c, whereas the range of K/p separation is extended to about 2.0 GeV/c (Fig. 12). In addition, electrons can be separated from pions and kaons up to about 350 MeV/c and 1.3 GeV/c, respectively.

5.3.3 Momentum resolution

For $p < 1$ GeV/c, the momentum and angular resolutions are dominated by multiple scattering in the beam pipe and layers of silicon sensors. The momentum resolution was estimated using Monte Carlo simulations of particle tracks (see Fig. 13). It is observed to increase from about 1.3% to 2.7% over the momentum range $p = 0.5 - 9.5$ GeV/c. Above 10 GeV/c the momentum resolution is expected to scale as $\Delta p/p \approx 0.3\% \times p/\mathrm{GeV/c}$.

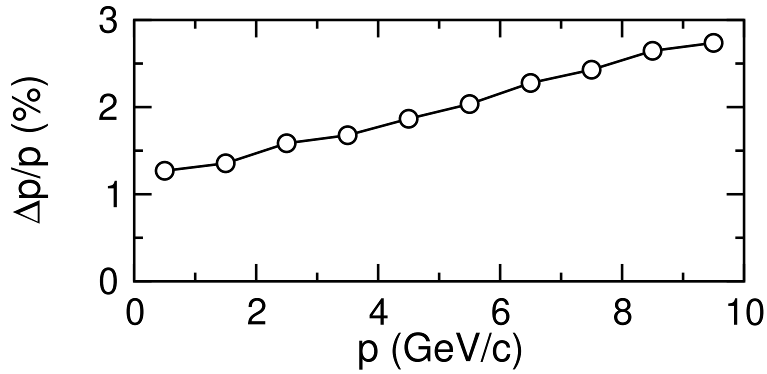

Fig. 13. The estimated momentum resolution for singly charged particles is shown as a function of the momentum.

6 Time-of-flight wall

The time-of-flight wall is constructed of Bicron [12] BC404 scintillator, which has good timing characteristics (a 1.8 ns decay constant) and a moderate attenuation length (1.6 m). Its wavelength of maximum emission (408 nm) is close to the wavelength at which the response of most fast photomultiplier tubes peak (420 nm). The scintillators are 200 mm high and have cross sectional areas of 8x8 mm^2. Photomultiplier tubes with fast rise time (= 1.8 ns) and high gain ($= 1 \times 10^6$) (Hamamatsu [13] R5900) which feature a segmented anode (4 8.8x8.8 mm^2 channels per unit) were used. The 2 x 2 design requires a complex light-guide geometry and mounting fixture (see Fig. 14). Two photomultiplier tubes are coupled via light guides to the end of four scintillators. The anode signals from the photomultiplier tubes are split into two components. One is digitized after a 400 ns delay using a FASTBUS 13-bit ADC (LeCroy 1881M) and the other is connected to a CAMAC leading-edge discriminator (LeCroy 3412), located close to the photomultiplier tube. The ECL output signals from the module are delayed using cable delay before being digitized using a FASTBUS TDC (LeCroy 1875A) operated with a sensitivity of 25 ps/channel.

Simultaneous measurements of the time and pulse height allow slewing corrections to be made, which are required to achieve time-of-flight resolutions better than 100 ps. The time information provided by the individual photomultiplier tubes is also used to determine the vertical position of the traversing particles. This measurement greatly enhances the capabilities for matching particle tracks reconstructed in the Spectrometer with the hits recorded in the time-of-flight wall. The timing information is lost, however, if more than two particles hit one scintillator segment. In many cases, this type of event

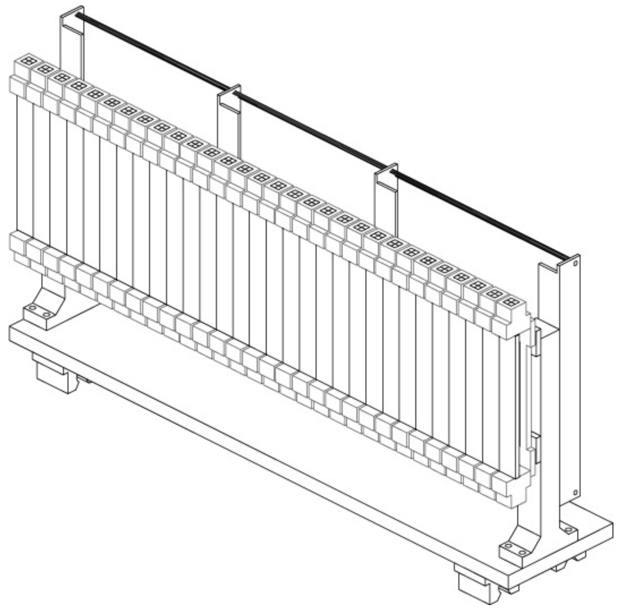

Fig. 14. Schematic drawing of the Time-of-flight wall.

can be recognized and identified by checking the consistency of the time difference between the photomultiplier tube signals and the ratio of their pulse heights. The time-of-flight wall is designed to keep the double-hit probability as low as possible. The segmentation of the time-of-flight sections is determined by the requirement that the average occupancy be less than 15% for a high-occupancy event with a charged particle density $dN/d\eta = 1000$ at $\eta = 0$.

The time and position resolutions of the time-of-flight elements have been studied in detail using sources and cosmic rays. The measured time-of-flight resolution is approximately 75 ps (1σ). The measured position resolution is 10 mm (1σ) for the reconstruction based on time differences and 37 mm (1σ) for the reconstruction based on the ratio of pulse heights. Two time-of-flight sections, each consisting of 120 scintillators, are currently installed, covering $0 < \eta < 1.24$.

6.1 Time-zero detectors

The time of flight is measured relative to a time signal generated by two time-zero (T0) Čerenkov detectors located at $z = \pm 5.3$ m. These two counters are each composed of four Bicron [12] BC800 Čerenkov radiators of 25 mm thickness and 50 mm diameter coupled to fast 50 mm diameter phototubes (Hamamatsu [13] model R2083). An intrinsic time resolution of 110 ps has been observed. These detectors are centered on a circle of diameter 151 mm around the beam line. The T0 counters also provide prompt information on the vertex position from the relative time between the two detector arrays with an accuracy of about 50 mm and may be used in the trigger logic to select only events which fall within a vertex range of $|z|$ <200 mm.

7 Trigger detectors

The PHOBOS experiment has three sets of trigger counters: the paddle counters, which serve as the primary event trigger [14], the Čerenkov counters, which produce the interaction vertex trigger, and the zero degree calorimeters [6], which are common to all RHIC experiments and serve as a true minimum bias trigger.

7.1 Paddle counters

The paddle counters consist of two planar arrays of 16 detectors each, made of BC-400 plastic scintillator. The arrays are positioned perpendicular to the beam surrounding the beam pipe at $z = \pm 3.21$ m from the nominal interaction point and subtend 94% of the solid angle in the range $3 < \eta < 4.5$. Trigger requirements based on the number of detectors that have fired and on the total energy deposited in each array can be set. These capabilities provide a flexible trigger that can be used to determine the event centrality [15]. Background events can be suppressed by requiring that a valid event has at least one hit in each array. More selective criteria can be set to favor more central events and further suppress background events from interactions of beam particles with residual gas molecules in the beam pipe.

7.2 Čerenkov timing detectors

Čerenkov trigger counters can also be used to reduce background events and to restrict the accepted range of vertex positions. These are two rings each consisting of 16 Lucite radiators placed at $z = \pm$ 5.5 m. The relative timing of the two arrays, which have intrinsic time resolutions of about 110 ps, will provide a fast, online cut on the vertex position. Setting a specific requirement for this time difference will allow for the selection of collisions occuring within $\pm$200 mm of $z = 0$.

The final set of trigger counters used in PHOBOS is the Zero Degree Calorimeters (ZDC's) used to detect spectator neutrons. The ZDC's are placed after the DX magnet where the two RHIC accelerator beam tubes separate at ±18.5 m from $z = 0$. Each ZDC consists of three calorimeters made of sandwiches of twenty two 5 mm thick tungsten converters and ribbons of twenty 0.5 mm diameter commercial grade optical fibers which sample the Čerenkov light. A bundle of all 4200 fibers is placed in front of a 50 mm diameter photomultiplier tube (Hamamatsu, Model R-239). Three modules are placed behind each other in order to collect about 98% of the neutral energy within a 3.1 μsr solid angle around 0°. Further details on these detectors may be found in Ref. [6].

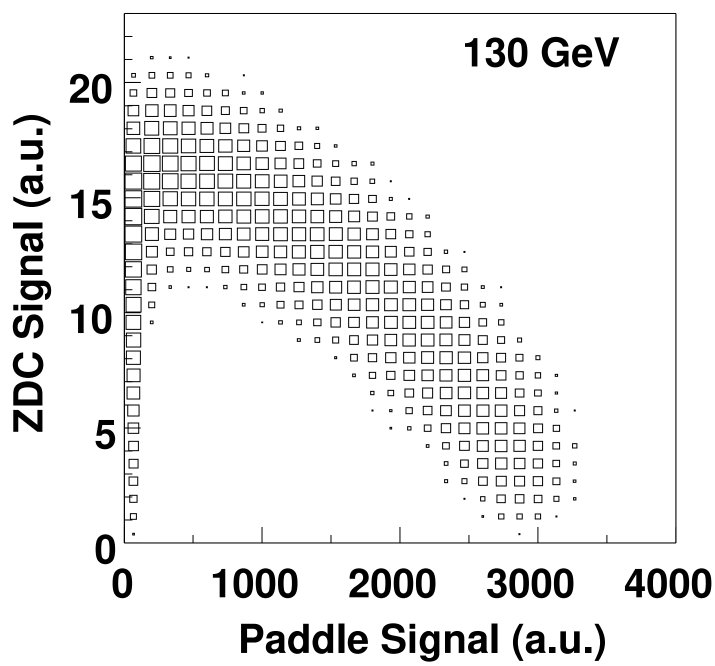

Fig. 15. Correlation between energy detected in the ZDCs and the paddle counter signal.

The ZDCs provide an experiment independent event trigger, which can be used during beam tuning and to cross correlate the results of the different experiments. A clear anti-correlation between the signal from the Paddle counters and the ZDC's is observed (see Fig. 15). For peripheral collisions, the neutrons are bound in charged fragments which are deflected by the DX magnets. This leads to a reduction of the ZDC signal. Therefore a small signal (few spectator neutrons) is observed for both central and peripheral collisions.

8 Detector surveys

The location of all active pads of the Silicon sensors was determined by a combination of optical survey of the individual detector modules, optical survey of the modules relative to the mounting frames, and optical survey of the frames in their final position within the PHOBOS coordinate system. The first survey step was performed on an optical survey station with an accuracy about 10μm in the plane of the sensors, whereas the last two survey steps attained an accuracy of about 100μm. All trigger counters and the TOF wall were surveyed optically in their final positions.

9 Electronics and data acquisition

The front-end electronics for the silicon detectors serves 135,168 channels: 56,064 channels in each of the two Spectrometer arms, and 23,040 channels in the Multiplicity and Vertex detectors. The front-end system has a uniform structure for all different types of Si modules. It uses the elements shown in Fig. 16. A detector module, composed of silicon sensors and front-end chips on a multichip module, connects via a short flex cable to a nearby front-end controller. The controller digitizes the event data and sends it via G-Link to a data concentrator, which collates the event data into serial streams and transmits them over optical fibers to the data acquisition system (DAQ) in the counting house.

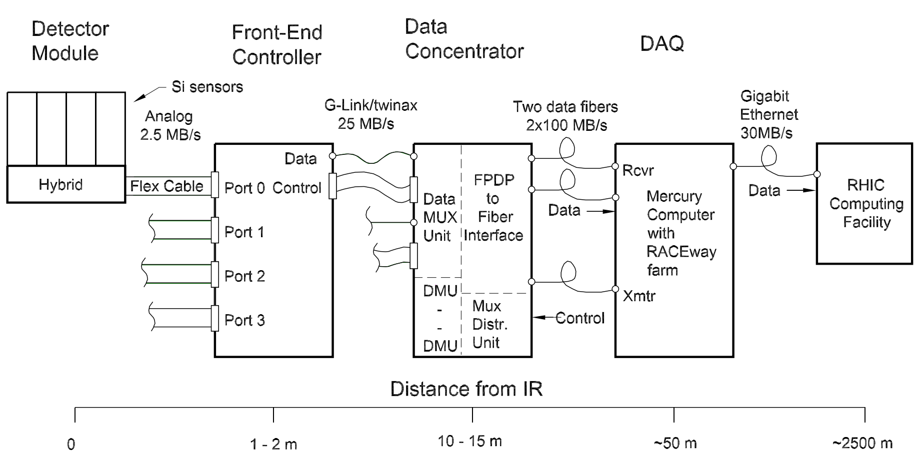

Fig. 16. Block diagram of front end electronics (FEE) and data acquisition system (DAQ).

A typical Vertex or Spectrometer detector module has two to four silicon sensors and their associated front-end chips mounted on a multichip module "hybrid", (see Sect. 4). For the front-end chip, a version of the commercially-available line of VA integrated circuits [16] was used, which has a dynamic range corresponding to 100 times the energy deposition of a minimum ionizing particle in the 300μm thick silicon sensors . The VA chip has a bussed, differential analog readout that allows several of the chips to be concatenated on one hybrid. This feature renders the connection requirements between hybrid and front-end controller independent of the number of chips per module and therefore uniform throughout the system. The Octagon and Ring modules, which contain only a single VA chip per module are connected to read-out boards which serve between 4 and 10 modules per board.

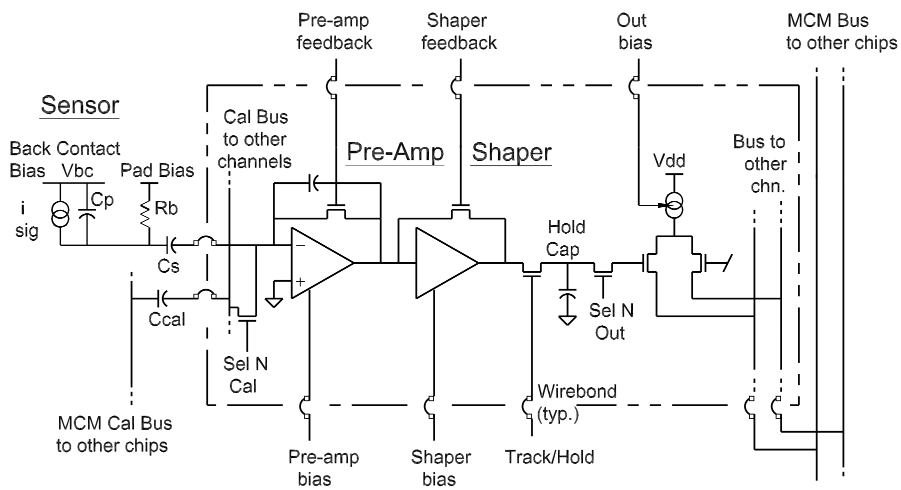

Fig. 17. Schematic of VA chip.

The VA chip contains a charge-sensitive pre-amplifier which integrates the detector signal current; the nominal integration time is 100 ns at 10 pF input load, and the decay time is set at about 50 μs. The PHOBOS silicon-sensors have a range of pad sizes corresponding to capacitances between 5 and 200 pF per pad. The preamplifier is followed by an RC-CR shaping stage (peaking time 1.1 μs) and a track-and-hold stage. During readout, an output control shift register sequentially selects the hold capacitor in each channel and connects it to a differential output stage which drives output currents onto the analog bus. The"Shift-out" from the output control shift register feeds the "Shift-in" input of the next chip. A second control shift register is invoked only during test/calibration. The calibration step input signal (0 to a maximum of 190 mV) is fed via an off-chip 2 pF calibration capacitor to an internal bus on the chip, and the shift register connects this bus to the input of each channel in turn.

The multichip modules use thick-film circuits fired on alumina substrates that provide good thermal conduction of the heat generated by the VA chips to the water-cooled frames. The circuits are composed of six layers: three signal layers on the top side, and on the bottom side a layer each for the two power rails ($V_{dd} = +2V, V_{ss} = -2V$) and ground. Two of the signal layers accommodate the 200μm-pad pitch at the control side of the VA chip, and the third carries a bus which connects all chips to the I/O connector, a 30-pin header, at one end of the substrate. Topside components include the VA chips and their associated biasing resistors and bypass capacitors, a calibration signal attenuator and insertion capacitors, and a temperature sensor. Bottom-side components are restricted to the 10kΩ series limiting resistors and 4.7nF/200V bypass capacitors that serve the back-contact electrode of each silicon sensor.

9.2 Flex cable

For connecting the detector modules to the front-end controllers, cables with a 30-conductor flat cable core and laminated copper foils on both surfaces for carrying the power rails and ground were manufactured. This composite cable provides controlled impedance for digital signals, good shielding for sensitive low-level analog signals, and a copper cross-section to carry the load currents with acceptable voltage drops. The cable is terminated at each end in a small, connector card assembly: a printed-circuit board which carries a 30-pin plug, shrouded header or, in the case of the port connector for the front-end controller, a right-angle through-hole header with strain relief.

9.3 Front-End Controller

The detector modules are controlled and read out by modules located about 2 m from the silicon detector. The module has four input ports; each port accommodates up to 1,472 channels split evenly between two readout strings. Because of their proximity to the detector, the front-end controller modules and their crate are custom-designed to meet tight spatial constraints. The front-end controller (FEC) is a 6U-high, 25mm-wide module composed of a signal board and a daughter board with power regulators. There is no crate backplane; the control signals and data are cabled directly from the back end of the signal board to the data concentrator. Low-voltage, DC power is distributed on a busbar system at the rear of the crate and is jumpered to the rear of the power board.

The FEC signal board is shown schematically in Fig. 18. It includes circuitry for eight readout strings - two per port. Each port provides back-contact bias for the silicon sensors, bias and control signals for the VA chips, and temperature monitoring. Each of the two strings provides a differential analog signal and a digital signal, "shift-out", which indicates that the last channel of the string has been read. The string circuit on the signal board contains a differential receiver, ADC and FIFO which can store two events worth of data. The string circuit also contains a built-in pattern generator for testing the data chain from the FIFO input, and a calibration circuit [17] which, in addition to its role of calibrating the analog front-end, tests the full functionality of the front-end beginning at the VA chips.

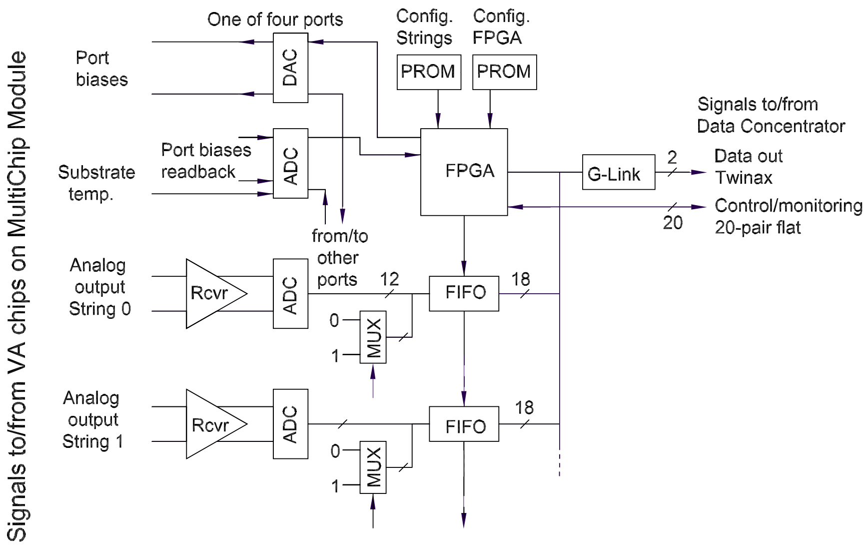

Fig. 18. Block diagram of FEC signal board - one port shown.

The front-end controller uses a field programmable gate array (FPGA) [18] to coordinate the activities of the module in each of four modes of operation: Set-up, Test, Calibration, and Run. At power-on, the FPGA's internal logic is configured from a programmable read-only memory chip (PROM). The configured FPGA then reads a second PROM containing information specific to each port, including the safe, initial bias values for the sensor and VA chips, and the number of channels per string. In the Run mode, the FPGA idles until receiving a 1.1μs-delayed version of the first level event trigger (L1d); the FEC sends a "Hold" signal to the VA-chips causing them to capture the peak of the channel signals. When the level two trigger signal (L2) is received, the FEC begins reading out the strings into their respective FIFOs, and upon completion the controller then unloads the FIFOs in sequence and appends a trailer block with parity bits. The event data is transmitted at a rate of 25 MB/s by a G-link interface over twin coaxial cable to the data concentrator.

Power for the FEC is conditioned by a number of regulators on the power board, which supply +5 V for the digital control logic, ±5 V for the analog circuitry, and a set of voltages for each of the four ports. The latter are generated by a 0 to +200 V regulator for the sensor back-contact bias, and by

± 2 V regulators for the VA-chip. Protection against front-end chip latchup is provided on a port-by-port basis.

9.4 Data Concentrator

The data concentrator multiplexes and collates the data from the front-end controllers into two bit streams for transmission to the acquisition system. It also receives the event triggers from the nearby trigger system and distributes these to the front-end system and counting room. All FECs are unloaded in parallel, and each controller transmits its data via G-Link at a rate of 25MB/s over a twin coaxial cable to a two-port Data Multiplexing Unit (DMU) in the data concentrator. The data from the two ports are multiplexed and stored in a FIFO. Under the control of the Multiplexor Distributor Controller (MDC), the DMU FIFOs are multiplexed to a common 32-bit bus using the FPDP protocol. Data on this bus are received by a FPDP/Fiber Interface (FFI) module in the same crate; this full-duplex module serializes the data and transmits them at 100 MB/s over an optical fiber to the counting house.

The three types of modules - DMU, MDC and FFI - in the data concentrator are custom designed; they are based on programmable gate array logic. The DMU has a G-Link receiver, FIFO and FPDP addressable interface for the data path. It also interfaces control and monitoring signals to and from the FECs over 20-pair flat cables. The MDC module provides the master function in a crate filled with DMU modules, and it prepares data (bias parameters for each of 4 ports in each FEC) for downloading to the front-end system. It checks record length and parity for data on the FPDP bus, and adds status information at the end of each record. The MDC's tasks are controlled by commands received over fiber from the data acquisition system; this fiber occupies the second port of the full-duplex FFI module.

9.5 Data Acquisition System

The Data Acquisition System (DAQ) is capable of accepting data from 150,000 silicon and 2,000 scintillation detectors channels at an event rate of 200 Hz, and sending the data over a Gigabit network to the RHIC central data storage system at a sustained rate of 30 MB/s. A significant portion of its computational effort is devoted to processing the raw data from the FECs to achieve common-mode noise correction and zero suppression of the data. The DAQ comprises: 1) 24 PowerPC-750 CPUs, all connected to a RACEway crossbar switch, 2) Host CPU: Themis USPIIi VME board with ULTRASparc 450 MHz processor, 1 GB of memory, 2 SCSI channels 40 MBytes/s, Gigabit Ethernet NIC, 3) 1 PowerPC-604 CPU. The total processing power is 330 SPECint95.

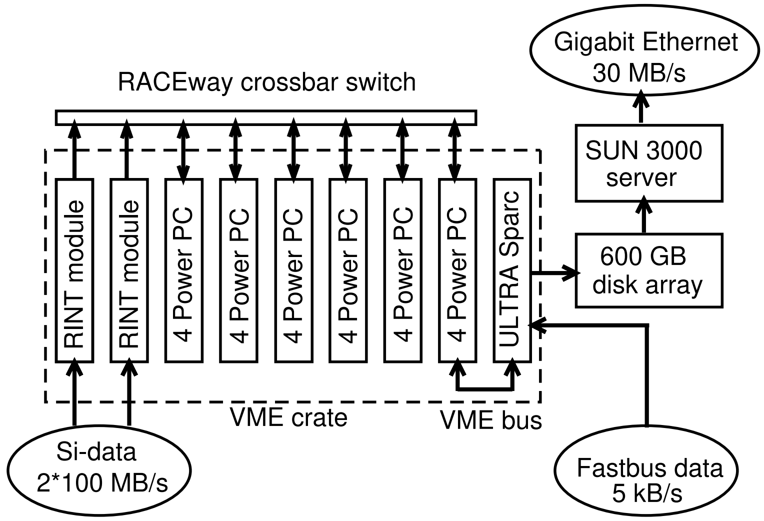

Fig. 19. Overview of the PHOBOS data acquisition system.

The structure of the DAQ is shown in Fig. 19. The data from the silicon detectors are received over two fiber optic channels at the rate of 100 MB/sec by two RINT modules, connected directly to the RACEway farm. They distribute data on-the-fly between 24 analyzing worker CPUs. When a worker CPU receives its dedicated portion of the event, it starts processing the data and, upon completion, sends a compressed buffer directly to the memory of the host UltraSPARC VME computer [19] (running Solaris OS) residing in the same VME crate. As soon as all CPU workers have finished sending their output data, the host constructs a ROOT [20] event object and streams it to the RAID0 disk array at maximum rate of 40 MB/s. The disk array has 2 host ports and 2 drive ports; this makes it possible to write to one disk from one host and simultaneously to read from the other disk to the other host. The second host port is connected to an UltraSPARC server that reads data files and sends them over Gigabit Ethernet to the RHIC Computing Facility. The measured sustained data-taking rate of the whole system is 30 MB/s.

9.6 Trigger logic

The data from the TOF spectrometer and the trigger counters are digitized in a FASTBUS crate and received in the DAQ crate using a custom-designed, VME module with Programmable Control and Data Ports (PCDP). One such module is programmed to function as a Level 0 trigger; a second module combines level one trigger (L1) logic and pre scalers; a third module functions as an Event Manager Master which distributes an 8-bit event number to two Event Manager Slaves to enforce event synchronization in the different subsystems.

The UltraSPARC VME computer distributes the recent events on demand to an online monitoring computer, which in turn distributes the events via

TCP/IP to more than ten online monitoring processes. The run control is done using ROOT scripts and a ROOT-based graphical user interface.

The entire PHOBOS trigger logic, including the Event Manager Master and Slave modules, is built using the general-purpose PCDP module. This VME module provides front-panel access for 16 differential ECL inputs and outputs and a 17-bit, differential TTL bi-directional port. The heart of the module is an in-system programmable logic array chip. The module has less than 20 ns propagation time and is used to generate first- and second-level triggers and fast clear signals, and to scale down input triggers. The dTTL port is used for event synchronization, alarm control and data transfer.

10 Summary

The PHOBOS detector was designed to perform comprehensive studies of global parameters of ultra-relativistic heavy ion collisions with almost complete coverage of the solid angle. The multiplicity of charged particles can be measured over the pseudorapidity interval $-5.4 < \eta < 5.4$ using an array of silicon-pad detectors arranged in an octagonal barrel geometry covering the mid rapidity region $|\eta| < 3.2$ complemented by six Ring detectors that extend the pseudorapidity range to $|\eta| < 5.4$. This detector system has been used both to measure charged particle multiplicities [1,3] and collective flow characteristics [21].

In a limited region of phase space ($0 < \eta < 2$) more detailed charged particle measurements can be performed by using the two arm PHOBOS tracking Spectrometer. Charged particles within this acceptance can be identified and momentum analyzed on the basis of energy loss in consecutive silicon pad detectors and the curvature of the trajectory in the magnetic field regions. These measurements allowed for the study of the anti-particle to particle ratios [2]. The particle identification in the high transverse momentum region is augmented by time-of-flight measurements. The vertex position of the collisions is determined using a dedicated Vertex detector having two layers of finely segmented Si detectors, as well as the first six layers of Silicon pad detectors of the Spectrometer arms, which reside in a near field-free region.

Event triggering and the determination of the centrality of the collision is obtained from two scintillator paddle counters. Measurements from these counters are augmented by the detection of the neutral spectator energy captured in two zero degree calorimeters. Such calorimeters are installed at all four RHIC experiments with the purpose of providing common trigger conditions to allow direct comparison of results.

The 135,168 Si detector channels are read out by front end electronics utilizing the VA pre-amplifier chip and custom fabricated control and data handling modules. The various scintillator and Čerenkov detectors are supported by commercial electronics modules. The data acquisition system utilizes 24 VME board mounted CPU's (Power PC) and an event distributing RACEway cross-bar switch to optimize the data acquisition rate. Further data validation and analysis is performed using the ROOT analysis framework.

The PHOBOS detector was successfully commissioned and used to measure $\sqrt{s_{NN}}$=130 GeV Au+Au collisions during the Year 2000 RHIC running period. Several measurements of particle multiplicity [1,3], particle/anti-particle ratio [2] and collective flow [21] have been carried out. The performance of the detector during this initial running period was essentially flawless. After the Year 2000 run, the second Spectrometer arm was fully instrumented and commissioned in the early part of the Year 2001 RHIC running period. The state of the PHOBOS detector described in this article reflects the configuration used in the Year 2001 running period.

11 Acknowledgments

The generous support of the entire RHIC project personnel, C-A and Chemistry Departments at BNL is acknowledged. We thank Fermilab and CERN for help in Silicon detector assembly. We thank the MIT School of Science and LNS for financial support. This work was partially supported by U.S. DOE grants DE-AC02-98CH10886, DE-FG02-93ER40802, DE-FC02-94ER40818, DE-FG02-94ER40865, DE-FG02-99ER41099, W-31-109-ENG-38. NSF grants 9603486, 9722606 and 0072204. The Polish groups were partially supported by KBN grant 2 PO3B 04916. The NCU group was partially supported by NSC of Taiwan under contract NSC 89-2112-M-008-024.

References

[1] B. B. Back *et al.*, (PHOBOS Collaboration), Phys. Rev. Lett. **85** (2000) 3100.

[2] B. B. Back *et al.* (PHOBOS Collaboration), Phys. Rev. Lett. **87** (2001) 102301.

[3] B. B. Back *et al.*, (PHOBOS Collaboration), Phys. Rev. Lett. **87** (2001) 102303.

[4] B. B. Back *et al.*, (PHOBOS Collaboration), Submitted to Phys. Rev. Lett. **88** (2002) 22302.

[5] 12th International Conference on Ultra-Relativistic Nucleus-Nucleus Collisions : Quark Matter '96, Proceedings P. Braun-Munzinger, H. J. Specht, R. Stock and H. Stöcker, Nucl. Phys. **A610** (1996) 1c-614c.

[6] C. Adler *et al.*, Nucl. Instr. Meth. **A461** (2001) 337.

[7] R. Nouicer *et al.*,(PHOBOS Collaboration) Nucl. Instr. Meth. **A461** (2001) 143.

[8] National Instruments, 11500 N Mopac Exprwy, Austin, TX 78759-3504, U.S.A.

[9] Heinz Pernegger, Nucl. Instr. Meth. **A419** (1998) 549.

[10] Oracle Corporation, 500 Oracle Parkway, Redwood Shores, CA 94065, U.S.A.

[11] H. Pernegger *et al.* (PHOBOS Collaboration) Submitted to Nucl. Instr. Meth. **A** (2001).

[12] Bicron, Inc., 12345 Kingsman Rd., Newbury, OH 44065, U.S.A.

[13] Hamamatsu Photonics, 314-5 Shimokanzo, Toyooka-village, Ivata-gun, Shizuoka-ken, 438-01 Japan

[14] R. Bindel, E. Garcia, A. Mignerey, and L. Remsberg, Submitted to Nucl. Instr. Meth. **A** (2001)

[15] J. Katzy *et al.* (PHOBOS Collaboration), Submitted to Nucl. Phys. **A** (March 2001) (QM2001 proceedings).

[16] E. Nygård *et al.*, Nucl. Instr. Meth. **A301** (1991) 506; O. Toker *et al.*, Nucl. Instr. Meth. **A340** (1994) 572; B. Alpat *et al.*, Nucl. Instr. Meth. **A439** (2000) 53; Integrated Detector & Electronics AS (IDEAS), Veritasveien 9, N-1322 Høvik, Norway, commercialized as VA-HDR.

[17] E. Griesmayer, H. Frais-Klbl, H. Pernegger, B. Wadsworth, J. Fitch, IEEE Trans. Nucl. Sci. **48** (2001) 1565.

[18] Xilinx Inc., 2100 Logic Drive, San Jose, CA 95124, U.S.A.

[19] Mercury Computer Systems, Inc., 199 Riverneck Road, Chelmsford, MA 01824-2820, USA.

[20] R. Brun and F. Rademakers, Nucl. Instr. Meth. **A389** (1997) 81.

[21] I. Park *et al.* (PHOBOS Collaboration), Submitted to Nucl. Phys. (QM2001) (March 2001)